Smart Materials and Structures

ACCEPTED MANUSCRIPT

Piezoelectric actuators with on-board sensing for micro-robotic applications

To cite this article before publication: Shivam Chopra *et al* 2019 *Smart Mater. Struct.* in press https://doi.org/10.1088/1361-665X/ab43fe

Piezoelectric actuators with on-board sensing for micro-robotic applications

Shivam Chopra[1], **Nick Gravish**[1]

[1]Department of Mechanical and Aerospace Engineering, University of California San Diego. 9500 Gilman Dr, La Jolla, CA 92093 USA

E-mail: ngravish@eng.ucsd.edu

Abstract. We present a piezoelectric actuator design with integrated position sensing for millimeter scale mobile robotics. Actuators are fabricated using the Smart Composite Microstructure (SCM) fabrication process which consists of laser micromachining and composite lamination. Electrically isolated strain-sensing regions of the piezoelectric material undergo identical motion as the actuation layers and thus directly sense tip deflection through the piezoelectric effect. We present the design considerations of strain-sensing piezoelectric actuators which can be made over a wide range of sizes and in both unimorph and bimorph configurations. These actuators demonstrate a linear relationship between the piezo sensor voltage output and the actuator tip to tip displacement when actuated over input bias voltages ranging between 25 – 200 V and frequencies from 10 – 250 Hz. We demonstrate the applicability of strain sensing actuators for microrobotic flying robots through wing-collision and wing-degradation experiments. Actuators enabled successful detection of instantaneous wing collisions when flapping near an obstacle. Furthermore, wing degradation through loss of wing area resulted in increased wing amplitudes which were observed in the sensor. Coincident actuation and sensing within microrobots represents a meaningful step towards closed loop control capabilities of microrobots using on-board sensors.

1. Introduction

Millimeter scale robots have application in search and rescue, exploration, and medical scenarios [1, 2, 3, 4, 5, 6]. Development of fabrication processes for millimeter scale robots have lead to methods such as smart-composite microstructures [7] and pop-up book assembly [8]. While many challenges of millimeter scale robotics have made great strides, including actuation and system design, other areas such as control and sensor development have lagged behind. Embedded sensing of joint angles and end-effector positions in millimeter-scale robots is a challenge due to the lack of off the shelf components and the tight dimensional restrictions on sensor placement and function. Thus, typical approaches to embedding joint sensing within microrobots use custom fabricated sensors [9] or require custom integration of off-the shelf components [10, 11].

Biomimetic sensors like ocelli and antenna have been custom made and integrated on these small scale robots [9] and stretchable sensors have been made to integrate with origami robots [12]. While ocelli and passive air dampers [13] have been used for roll-pitch detection, halteres act like biomimetic gyroscopes [14]. Off the shelf components like optical flow detectors [15] for motion detection/obstacle avoidance, magnetic compass for heading direction, cameras for gaze stabilization [16] temperature and chemical sensors for search operations [14] have also been proposed for flapping wing robots. Optical mouse sensor and MEMS gyroscope (off the shelf) have been integrated for 2-D position and angular heading in legged robots [10].

Piezoelectric actuators have been widely used for driving millimeter scale robots (Fig. 1) because of their ability to produce very accurate, high bandwidth and high force motion due to high power density and intrinsic stiffness [17, 18, 1, 19]. The planar machining and lamination process of fabricating piezoelectric actuators enables easy customization of size, stroke, and force requirements for robot applications [18]. Off the shelf actuators capable of driving milli-scale robots are commercially not available.

Position sensing methods for actuators that use off board sensors such as high speed cameras [20] or displacement sensors [21] are not appropriate for autonomous operation. Strain sensing in piezoelectric actuators has been proposed many times for example using electrical bridge circuits [22, 23], charge/voltage feedback [24], and combinations of charge based and capacitance based position measurement [25]. Almost all these methods

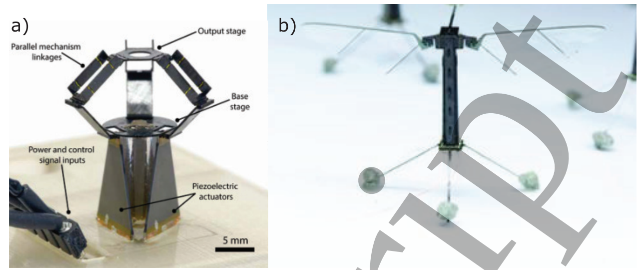

Figure 1. Examples of microrobots using piezoelectric bending actuators (a) Milli-Delta robot [4], (b) RoboBee [20].

either have a restricted range of operational frequencies or require additional sensing electronics. There are methods [26] by which the piezoelectric patch is attached to a specific area of a structure to sense the deformation but in most cases the process of fabricating actuators needs to be modified which in turn affects the actuation performance. A method [27] was proposed where a sensing layer was integrated into the actuator on the same piezoelectric layer. One electrode between the actuation and sensing regions acted as a ground, shielding the sensing from the high voltage input to the actuator. This method however is only applicable for unimorph actuators and resulted in less efficient actuation. Recently, concurrent sensing [28] on the actuator was studied without the use of any external sensing elements. Sensing is proposed based on the theory that motion of the actuators causes varying strains on the surface of the piezoelectric material, which, via the direct piezoelectric effect result in a current proportional to the actuator velocity. This method was successful in implementing closed-loop control of a micro-robotic limb and can be readily adapted to previously developed actuators.

A current focus in mobile robotics is towards multi-modal locomotion capabilities [30] and operation in complex and variable environments [31]. Recent research on a flapping wing flying robot demonstrated capabilities to transition from air to water [32]. Transitions between locomotion modes require precise adjustments of limb movements and sensing of the loads on limbs so as to adjust actuation accordingly. To achieve closed loop control in millimeter scale robots, on board sensing is needed for the robots to be driven in real world conditions.

In this paper, we propose an on-board strain sensor embedded on the piezoelectric actuator which can detect the wing or leg stroke amplitude of the robot in real time. This sensor has been successfully tested to detect

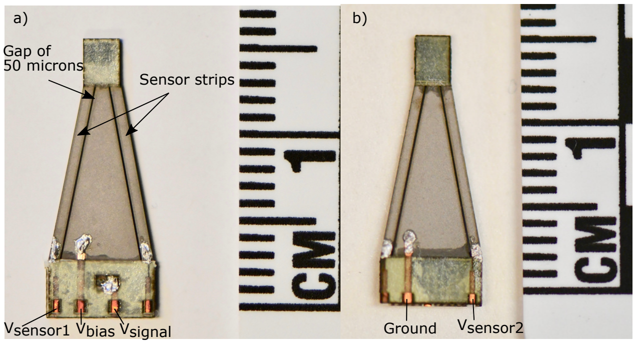

Figure 2. (a) Front view of the actuator, showing the gap of 50 μm and the electrical connections (b) Back view

perturbations like an obstruction in wing motion. Further it was experimentally verified that it can detect a change in wing stroke amplitude when the wing is cut. The actuator is made with piezoelectric sensor elements (PZT) on two sides using the Smart Composite microstructures (SCM) fabrication technique [7]. This actuator builds upon the work already done [17, 18] with additional steps for the sensor. Everything is cut on the same layer of PZT, so this method does not need any manual assembly and the thickness of the actuator remains the same. The strain sensors have the capability to detect any change in the actuator motion or in the assembly attached. The actuator was tested on different frequencies and different input voltages and the results were noted and verified with a displacement sensor.

2. Design and fabrication

2.1. Actuator Introduction

We fabricate bimorph actuators that have a single layer of piezoelectric material (PZT-5H) on each side of a central conductive carbon fiber layer. The general fabrication process for such actuators has been previously described [17]. A bimorph actuator [17, 18, 19] has three electrical connections, two for top and bottom PZT layers and one which connects to the central carbon fiber for access to the other electrodes of the PZT layers. The bimorph proposed here has two sensing layers of PZT which run along the side of the actuator (Fig. 2 and Fig. 3). The sensor strips are separated by a 50 micron gap to minimize electrical coupling while still being in mechanical contact with the actuator so that the sensors detect any motion the actuator experiences. The gap acts as a parallel plate capacitor with capacitance C inversely proportional to the gap width t. To minimize this electrical coupling we started with the minimum gap possible (10 microns) and sequentially increased the gap size until the electrical coupling between the actuator and sensor became sufficiently small. As the strain strips are fabricated on the same PZT layer, there is little manual assembly required.

2.2. Design overview

We propose to modify the pre-stacked actuator fabrication process of Jafferis [17] to integrate electrically isolated sensing regions. The actuator proposed is 0.65 mm thick and 17 mm in length and has two layers of PZT-5H 127 μm thick. PZT for this thickness is easily available and the FR4 thickness should be equal to the PZT (Fig. 4g) and all other materials have been chosen based on easy availability and least thickness. A primary design challenge for sensor integration is that the sensor regions must be electrically decoupled from the high-voltage actuation signals, but must be mechanically coupled to the bending motions of the actuator.

The fabrication process consists of laser machining layers of the actuator's constituent materials, and thus there are connectivity restrictions that must be upheld so that the layer does not fall apart during the lamination alignment step [33]. For instance, locating the sensing regions in the middle of the actuator would violate fabrication rules for SCM components because there would be no way to electrically decouple the PZT layer after alignment and lamination. For these reasons we have chosen to locate the sensing regions on the sides of the actuator as shown in Fig. 3. The central carbon fiber layer can then be cut for electrical isolation during the first cutting stage and yet mechanical coupling is still maintained by support bridges between the piezo sensor and actuator ends (Fig. 4).

The width of the sensing strips are chosen to be 0.68 mm and this width represents a trade-off between the sensors sensitivity, and it's effect on increased weight and stiffness. Piezoelectric sensor strips for different widths were tested over the actuator deflection described in this paper. Sensor strips with increasing width had higher voltage output under the same deflection. The bending stiffness of the actuator is modeled as a bending beam, with stiffness proportional to $\frac{bt^3}{l^3}$, where b is the width, t is the thickness and l is the length of the beam. Since t and l remain the same for our actuators with and without sensors, the only changing parameter is b which we have increased by exactly 25% resulting in an approximately 25% increase in the stiffness.

2.3. Fabrication

A 355-nm pulsed laser system was used (2 W output @20 kHz) to cut each layer with special consideration to cut PZT (PZT-5H) so it does not lose its dielectric strength. This involves first cutting all of the way through the PZT with a high number of laser passes at low power to avoid dielectric breakdown, then using a high power laser setting to melt the top edges of the cut. This process has been described thoroughly in Jafferis [17]. Each layer is cut with four 1.6 mm holes for pins. The fabrication steps are as follows:

1) Two layers of FR4 (glass fiber composite polymer)

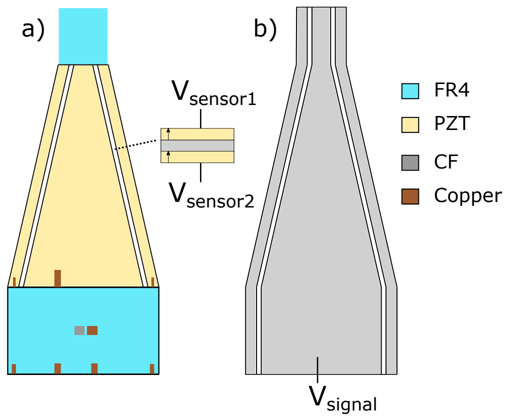

Figure 3. (a) Showing the cross section of the sensing strip (b) Carbon fiber layer of the actuator showing the cutouts for no electrical coupling between the actuating and sensing region

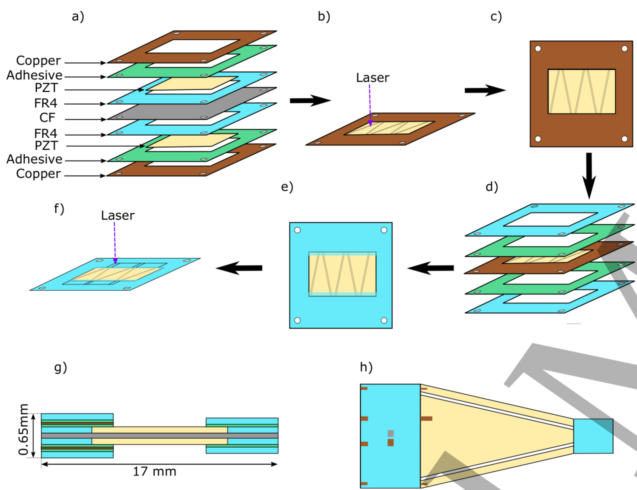

Figure 4. (a) - (f) Fabrication process from raw materials to the final actuators. (a) Each layer is cut using the laser and laminated in a weighted and heated press, (b) Partial release using the laser so that only the PZT is released (c) Laminate after release (d) Lamination is done again with FR4 bridge so that the sensor strips are held together (e) Final laminate (f) Final release (g) Side view of actuator. (h) Front view of the actuator

are cut with a rectangular hole in the middle to fit the rectangular PZT layers. The carbon fiber layer with an uncured epoxy resin embedded in it is cut with cutouts for sensing strips so that the fibers with the sensors do not electrically connect with the fibers of the actuator. Two layers of copper shim (25 μm) are cut for connections which would be adhered to the other layers using two layers of thermal adhesive (Dupont Pyralux) which is also cut exactly like the copper layer

2) These layers are stacked together (Fig. 4a) in a jig with 4 holes with Pacopad (Pacothane Technologies, Wincester, MA) on both top and bottom for equal distribution of pressure. A custom-made temperature-controlled heat press was used to press the laminate for 2 hours at 350 F under a pressure of 30 psi. After

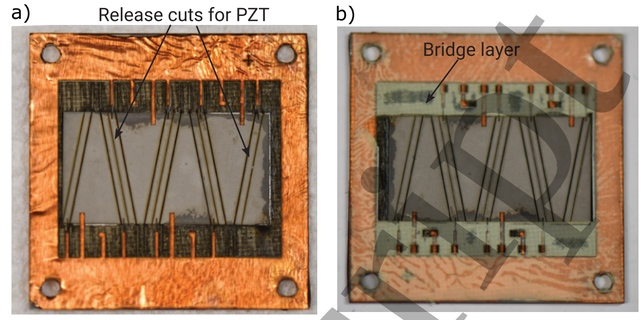

Figure 5. (a) The front view of the laminate after step 3 (b) Front view of the laminate after adding the bridge layers i.e step 4

lamination the laminate is removed from the heat press and placed on a slide under the laser cutter. The laminate is aligned on the laser and the release cuts are performed for PZT (Fig. 4b). Release cuts consist of laser cutting away all of the remaining material that attaches the actuator to the surrounding laminate. Once this material is removed the actuator is released from the laminate and can be removed. Release cuts consist of two power settings. First the low power cut is done for thousands of passes and then high power edge treatment is done [17]. A cut-through mark is made for alignment of top and bottom layers in the stack. The laminate is then flipped and the step is repeated for the other side. This step is done before FR4 bridge layer lamination and final release (steps 4 and 5) because we want the sensing region to be in mechanical contact with the actuating region while ensuring electrical isolation between these two regions.

3) After the release, the laminate is cleaned ultrasonically so that there is no residue in between the sensing and actuating parts. Additionally we remove any remaining residue using a fine microbrush under a microscope.

4) A layer of FR4 is cut which acts as a bridge holding the sensing and actuating layers together. The laminate is again put in the laminating press along with the bridge FR4 layers and Pyralux layers on both top and the bottom of the laminate (Fig. 4d-e, Fig. 5). A new Pacopad is used on both sides so that this layer is adhered well to the laminate. The laminate is again pressed for two hours exactly similar to what was done in step 2.

5) For the final release the laser is aligned with an alignment cut-through hole that was made in step 3 and raster slots are made for electrical connections to the carbon fiber in the middle. Finally the FR4 release cuts(Fig. 4f) are done to fully release the actuator.

6) The actuators are ultrasonically cleaned again and conductive epoxy is applied using a micro application probe to connect the copper with the PZT. Finally the

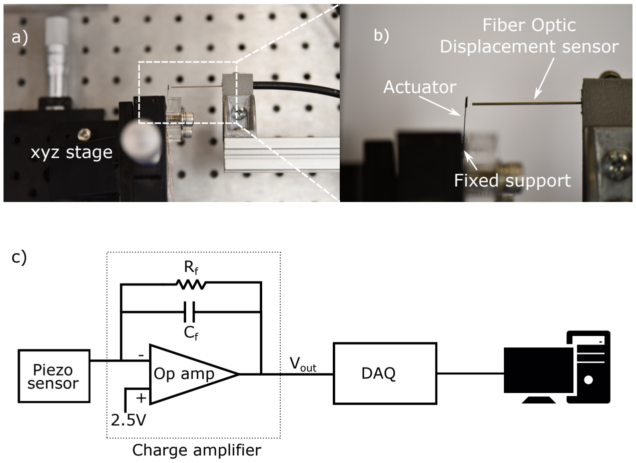

Figure 6. (a) Testing setup used for experiments with the actuator held three axis stage and a displacement sensor probe (Philtec) is held near the tip (b) zoomed in version (c) block diagram showing the signal conditioning of piezo sensor

copper conducting terminals are soldered to 40 gauge wire which are attached to a high-voltage amplifier.

The fabrication process takes approximately 12 hrs and for the actuator size studied in this paper yields 4 actuators with sensors.

3. Experiment setup

We tested sensing and actuation performance of actuators under several conditions including self-excited actuator motion, externally generated actuator motion, and fixed actuator strain excitation. The actuator is designed in a unipolar drive configuration [1] where a constant bias voltage, V_B, is applied to the top layer of the actuator, and the bottom layer is held at ground such that each piezoelectric layer is under a positive field with respect to polarization direction to prevent de-poling [1] of PZT. A sinusoidal voltage signal,

$$V_s(t) = \frac{V_B}{2}\sin(2\pi f t) + \frac{V_B}{2} \tag{1}$$

is used to drive the actuator (where V_S is the signal applied to the central carbon fiber layer such that $V_s \in [0, V_B]$). For these experiments the bias voltage V_B ranged from 25 V to 200 V. We tested actuators over a frequency range relevant for millimeter scale robots $f \in [10, 250]$ Hz. Both the output voltages are generated using a PCI-DAQ card (National Instruments) and amplified 25x using TD250 - 6 Channel 250V amplifier (PiezoDrive).

The output of the piezo sensor has to be passed through some signal conditioning because of its high output impedance [34]. Here an op-amp (LM6132) is used in a charge amplifier configuration with RC time constant chosen to match the working range of actuation frequency. However due to the property of piezoelectric material to leak charge, it is impossible to measure static deflections and their is poor performance at lower frequencies [34]. The output from the charge amplifier is then read into the DAQ (Fig. 6c). The actuator is mounted on a three-axis micrometer stage (0.001 inch resolution) fixed to a vibration reducing optical table (Fig. 6a,b). The probe tip of a fiber optic displacement sensor (Philtec D21) is placed approximately 2 mm from the actuator tip with a reflective piece of copper foil adhered to the actuator tip to increase displacement resolution. As this sensor works on the principle of optical reflection a clean and reflective surface would increase sensitivity. This sensor works in one of two possible sensing modes, close mode and far mode. The close mode has better sensitivity but the working distance is very small and so this can't work for the high stroke lengths of the actuator, thus we chose the far mode for sensing. We calibrated the fiber optic sensor by translating the micrometer stage and measuring fiber optic sensor voltage and using a cubic polynomial to calibrate actuator tip displacement δ and fiber optic sensor voltage V_{FO}.

The sensing layer voltage output from the piezo sensor and the displacement sensor are read at the same sample rate in Labview. For every value of frequency and amplitude the data is collected for 5 seconds and saved as a data file. The process is automated to collect data at each value of frequency ($10-250$ Hz in 10 Hz intervals) and amplitude ($25-200$ V in 25 V intervals). The raw data for both the philtec and the piezo sensor is sinusoidal (Fig. 7a) with no filtering required. Using the raw data the peak to peak voltage out of philtec and piezo sensor are calculated by finding the difference between the maxima and the minima of each of the sinusoidal curves (Fig. 7b).

4. Results

4.1. Self-excitation experiments

Self-excitation experiments consisted of driving the actuation layer with varied signal voltage, V_S, and measuring the tip displacement through the fiber optic sensor probe (Philtec) and the strain-sensing layers. We observed that with an increase in V_S, the amplitude of both the strain-sensing layer voltage and the fiber optic sensor increases (Fig. 7a) indicating that the piezoelectric sensors is sensing the increase in displacement correctly. When the actuator is run for a frequency sweep from $10-250$ Hz at different peak to peak amplitudes from $25-200$ V, we see a rise in the sensor output with a rise in the input voltage and as seen on the displacement sensor plot, the peak to peak displacement remains constant (Fig. 7b) for all the frequencies (the actuator resonant frequency is much higher than 600 Hz).

The piezoelectric sensor can be modeled [34, 35] as an electrical equivalent of a charge generator in parallel with a capacitance C_p, equal to the capacitance of the sensor and parallel to internal resistance R_p, through which the charge

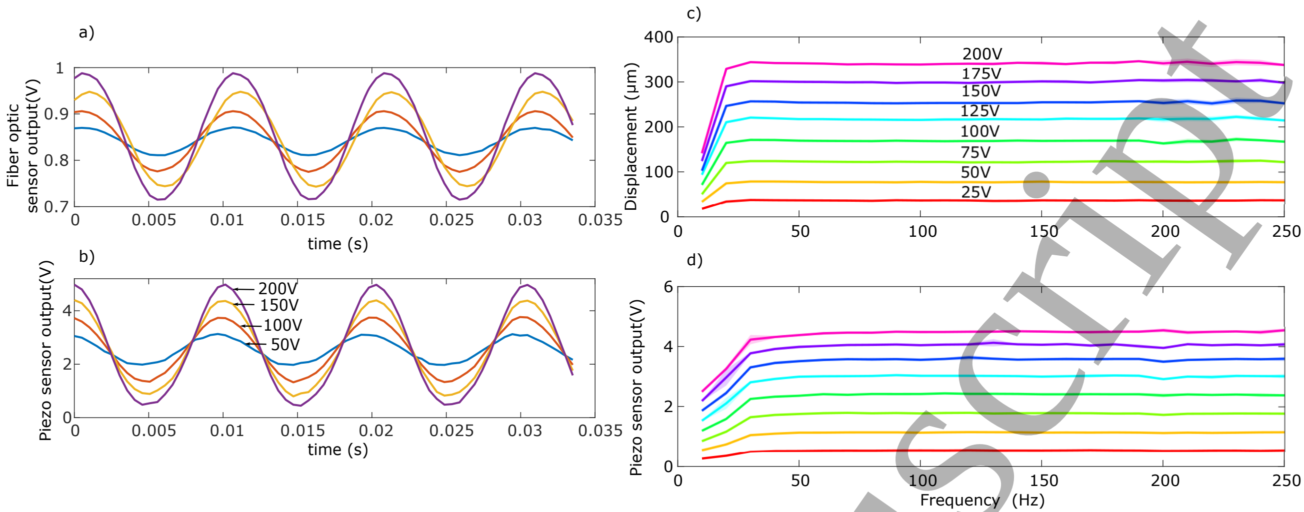

Figure 7. (a) - (b) show representative cycles of raw data outputs from (a) Philtec and (b) piezo sensor which are generated for a sine wave input of 100 Hz and different peak to peak amplitudes (50 V, 100 V, 150 V, 200 V). (c)-(d) show the varying amplitude of the (c) displacement from the Philtec and (d) piezo sensor output for 5 trials. Driving frequency varied from 30 Hz to 250 Hz and peak to peak amplitudes varied from 25 V to 200 V.

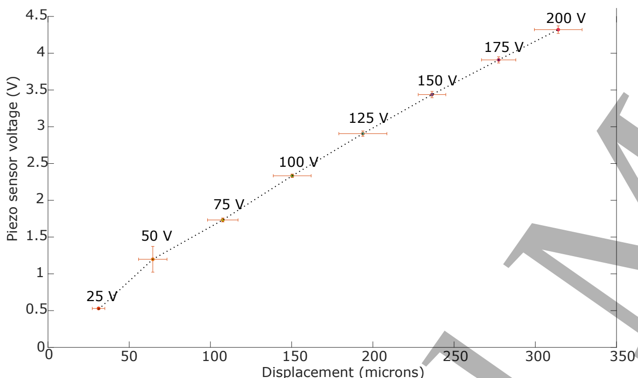

Figure 8. Voltage out of the sensor on actuator vs displacement in microns. Each point on the plot is a mean of the the data for 6 actuators which is generated by taking the mean of the data for a constant input voltage from Fig.7 from 30 Hz to 250 Hz. The error bars show the standard deviation for the 6 actuators.

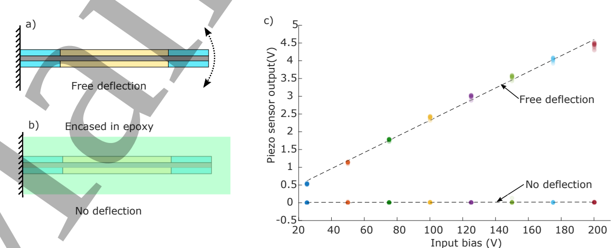

Figure 9. (a) Schematic showing the actuator in free deflection and no deflection by covering in epoxy (b) Plot shows the voltage output from the piezo sensor at different input bias voltages (25 V - 200 V), each point on the graph represents the voltage output at a particular frequency ranging from $10-250$ Hz in multiples of 10. The voltage outputs at these 25 points at each input voltage is averaged and fit using line regression. The plot shows clear difference in the slope of free deflection and the no deflection

gets leaked. As described in [34], the transfer function $H(\omega)$ of the circuit in frequency domain is,

$$|H(\omega)| = \left| \frac{j\omega R_F C_F}{1 + j\omega R_F C_F} \right| = \frac{\omega R_F C_F}{\sqrt{1 + (\omega R_F C_F)^2}} \qquad (2)$$

where R_F and C_F is the resistance and capacitance connected in parallel to the charge amplifier respectively. This function represents high pass filter characteristic with a cutoff frequency,

$$\omega_c = \frac{1}{R_F C_F} \qquad (3)$$

As now the circuit acts as a high pass filter the output data shown has lower amplitudes at lower frequencies (10 - 30 Hz). We observe that the working range of these actuators should be above 30 Hz and the peak to peak amplitude below 250 V as it has been mentioned in previous work [17, 18] that the dielectric breakdown for the actuators we are using is 3.7 V/μm and have been efficiently tested in the range of 0 - 2.2 V/μm. The maximum peak to peak amplitudes for frequency sweeps is 200 V to prevent cracking of the PZT. We tested 6 actuators (from two separate fabrication batches) and each actuator is passed through 5 trials of frequency sweeps at different amplitudes. The voltage displacement curve for all 6 actuators was plotted and it shows a linear relationship (Fig. 8). Constructing a fit of this slope results in a calibration mapping between sensor voltage and displacement.

4.2. Capacitive coupling measurements

In this experiment, we restricted actuator movement (Fig. 9a) by encasing the whole actuator in epoxy (Loctite Heavy duty) to determine the influence of electrical coupling on the strain sensor measurements. The actuator is actuated similar to the self-actuation experiments and the data out of the piezo sensor is recorded. When the actuator is in epoxy it cannot bend and ideally we should not observe any sensor voltage. Self-excitation experiments were done before and after applying the epoxy (Fig. 9) and the observations indicate clearly that coupling effects are minimal compared to the sensor voltage magnitude under free deflection. After fitting a linear regression plot for the data, it is found that the slope for the free deflection is 0.02271 ± 0.00147 (95% confidence bounds) and for the epoxy encased experiment we find a slope of zero. This experiment supports our observation that sensor voltage is primarily a function of tip displacement and not actuation voltage.

5. Demonstration of sensing in microrobot applications

Mobile micro-robots that fly, run, or swim often rely on limited or no onboard sensor feedback during operation because of size constraints and lack of off-the-shelf components. For example, the flying microrobot RoboBee [20] is capable of stable controlled flight [20], landing on surfaces (vertical and inverted) [36], and multi-modal locomotion (flight and swimming) capabilities [31] all through the use of external sensors. Incorporating onboard strain sensors into wing actuation will aid in moving towards onboard flight control of this robot.

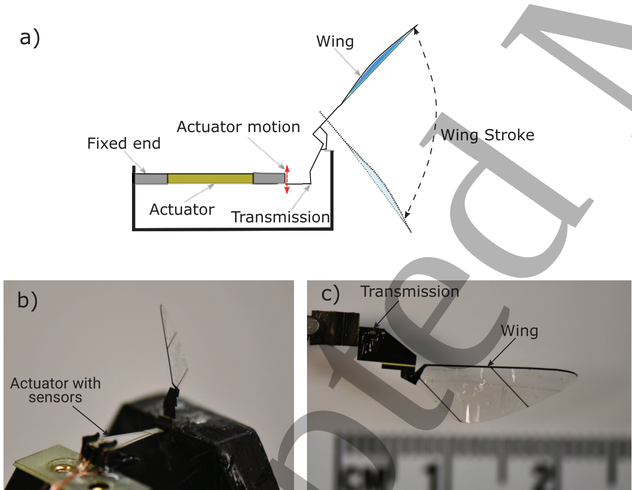

Figure 10. (a) A schematic showing the experimental setup for the demonstration of sensing experiments (b) Actuator attached to the wing transmission setup with one end and with the other end fixed (c) Wing-transmission setup used for applications

5.1. *Obstruction while flapping*

Flapping wing flight near obstacles is a necessary function for flying microrobot applications such as inspection and artificial pollination [37]. Wing perturbations can be highly destabilizing during flight and one strategy that has evolved in insects and incorporated into robots is the use of passive non-linear hinges to stabilize against wing perturbations [38]. However, the ability to detect wing perturbations in real-time through sensor feedback has not been demonstrated. Here we perform experiments to illustrate the applicability of onboard wing position sensing to detect a prescribed wing collision.

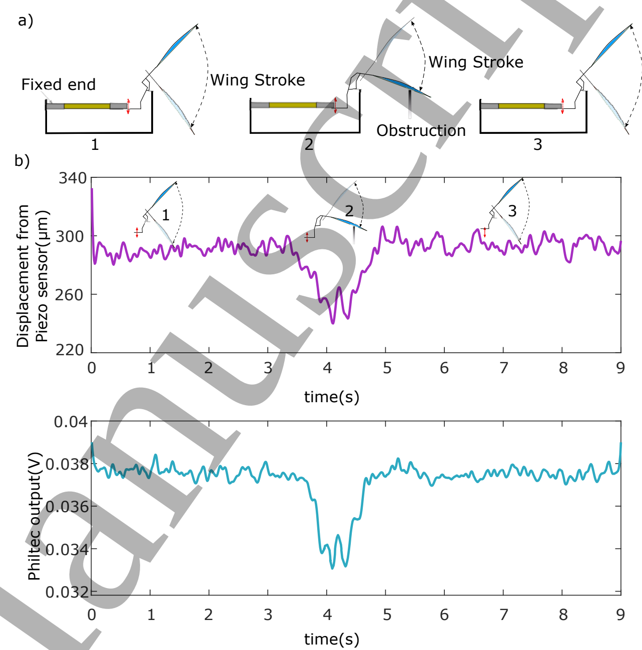

Figure 11. (a) Obstruction while flapping where 1 is before obstruction, 2 is during obstruction and 3 is after obstruction (b) top subplot shows the displacement measured from the piezo sensor (calculated using the data from Fig.8 and the voltage output from the piezo sensor) for 10 seconds of the experiment and the bottom subplot shows the voltage output of the Philtec

We attach an actuator to a microrobotic four-bar transmission [39] which drives the rotational motion of a microrobotic wing (Fig. 10). We drive the actuator a frequency of 100 Hz and bias voltage of 200 V. A displacement sensor (Philtec) probe is directed at the bottom side of the actuator and provides direct measurement of the actuator tip displacement, and thus the transmission input displacement. We also measure the sensor voltage from the actuator. While the wing is flapping, a thread under tension attached to a 3 axis stage is brought near the wing such that the wing strikes the thread for several seconds and then the thread is removed. We observe the process using high-speed video as well. The displacement sensor and the piezoelectric sensor both clearly indicate a decrease in peak-to-peak voltage upon wing collision (Fig. 11). This decrease is sustained during the wing collision duration after which the wing output returns to it's normal amplitude and the sensor readings do so as well. The four-bar transmission has relatively low serial compliance as that would require buckling of the Kapton hinges [40], thus real-time measurement of the sensor tip displacement are good indicators of the wing

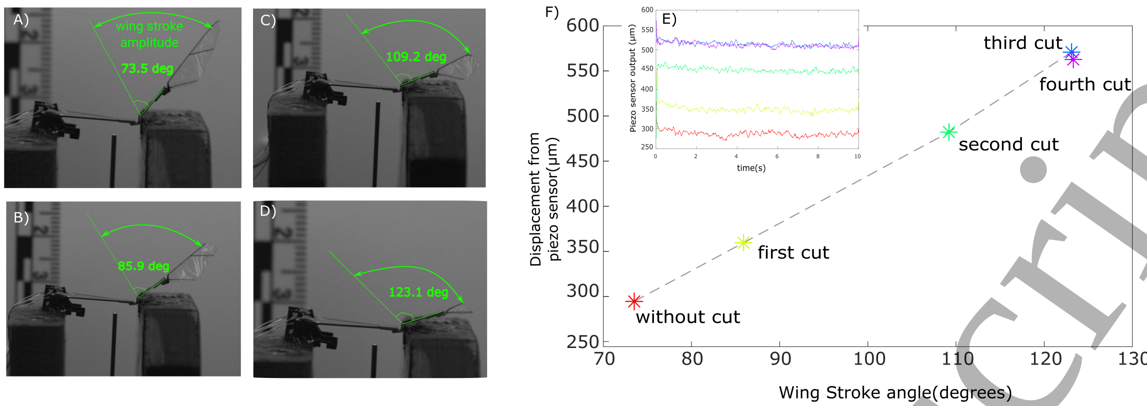

Figure 12. (a) - (d) Sequence of images from the high speed camera with decreasing wing length and increasing angles (e) shows the displacement measured from the piezo sensor vs time for 5 different wing lengths (f) Plot shows the displacement from piezo sensor vs the wing stroke angle.

stroke position as shown in this demonstration.

5.2. Detection of wing damage

In addition to needing to detect instantaneous changes in wing amplitude due to collisions, we may also need to make long term adjustments to actuation signals to compensate for wing damage. For instance, flying insects flap their wings close to obstacles at high frequencies and suffer wing damage over the course of their lives [41], which reduces flight performance and requires kinematic compensations [42]. Flapping wing robots can also experience such wing degradation through collisions with the ground during a crash, or while flapping near obstacles for many cycles in flight. Flapping wing microrobots are designed to flap their wings at resonance [43] and thus loss of wing area may change the optimal frequency which produces the highest wing amplitude. Thus there is a need for detecting wing area loss over microrobot lifetime so that proper actuation compensation can be performed (modulating frequency or amplitude). In these experiments, we demonstrate the ability to detect wing area loss through wing damage by sensing the output from the piezo sensor embedded in the actuator.

Similar to the setup in section 5.1 we oscillate a wing at normal flight parameters and measure output displacement using fiber optic sensor, onboard piezoelectric sensor, and high speed video. In between flapping observations we cut material away from the distal region of the wing that decreases the wing area. We observe in high-speed video that after each area decrease the wing amplitude increases since the wing drag resistance and inertia are reduced. Furthermore, we directly observe this wing amplitude increase by measuring the the peak to peak sensor voltage from our onboard strain sensors. We observe a linear relationship between wing flapping amplitude and sensor peak to peak amplitude (Fig. 12). Similar to the results of section 5.1 these observations demonstrate the capabilities of observing wing resistance variation which would be useful for control compensation as microrobots suffer damage in operation. The linear agreement between wing output angle and sensor voltage again confirms that the wing transmission has low serial compliance and sensing wing position through actuator deflection is a feasible method for closed-loop wing actuation.

6. Conclusion

In this work we have presented an actuator with embedded sensors capable of sensing the strain under actuation due to the piezoelectric effect. This sensing method can be easily integrated into previous actuator fabrication methods with only minor changes in the fabrication process for general bimorphs. Data output from the piezo sensor has been compared with a commercial displacement sensor and the displacement vs voltage output plot shows an approximate linear relationship. Applications were demonstrated by using this actuator with a wing transmission setup of a flapping wing robot and varying the loads. Wing collision experiments demonstrated the detection of wing collision during flapping wing motion. Furthermore, wing degradation experiments were successfully done to validate the sensors detection of wing angle change in real time. The poor performance at low frequencies is a downside to these sensors and presents limitations on their usage. To compensate for low frequency performance the time constant of the circuit for the charge amplifier can be made higher, but that would potentially increase the noise in the circuit. Thus, actuators with embedded strain sensing are extremely well suited for microrobotic applications in which rhythmic motion needs to be generated and sensed (such as actuating robot legs or wings). However, these sensors may not be suitable for force sensing when low frequency and constant forces need to be detected.

Closed loop positioning is needed for future microrobot control autonomy and on board sensors with piezoelectric actuators would be a valid choice for achieving this. In our applications for sensing the position of the wing in flapping wing robots, we have successfully demonstrated detection of wing angle changes in realtime, and this will enable future work on closed loop feedback of microrobot appendages during locomotion. Further work additionally will explore miniaturization methods for the sensor region on the actuator for better efficiency of the actuator. Further on-board signal conditioning would aid in achieving complete autonomy along with real time tracking of the limbs. These sensors can be used in many other applications like studying the contact mechanics of the limb of a terrestrial robot.

References

[1] Michael Karpelson, Gu-Yeon Wei, and Robert J. Wood. Driving high voltage piezoelectric actuators in microrobotic applications. *Sensors and Actuators A: Physical*, 176:78–89, apr 2012.

[2] E. Steltz, M. Seeman, S. Avadhanula, and R.S. Fearing. Power Electronics Design Choice for Piezoelectric Microrobots. In *2006 IEEE/RSJ International Conference on Intelligent Robots and Systems*, pages 1322–1328. IEEE, oct 2006.

[3] Andrew T Baisch, Onur Ozcan, Benjamin Goldberg, Daniel Ithier, and Robert J Wood. High Speed Locomotion for a Quadrupedal Microrobot. 2014.

[4] Hayley McClintock, Fatma Zeynep Temel, Neel Doshi, Je-sung Koh, and Robert J. Wood. The milliDelta: A high-bandwidth, high-precision, millimeter-scale Delta robot. *Science Robotics*, 3(14):eaar3018, jan 2018.

[5] Yun Seong Song and M. Sitti. Surface-Tension-Driven Biologically Inspired Water Strider Robots: Theory and Experiments. *IEEE Transactions on Robotics*, 23(3):578–589, jun 2007.

[6] Nobuaki Kawahara, Takayuki Shibata, and Takanari Sasaya. In-pipe wireless microrobot. volume 3834, pages 166–171. International Society for Optics and Photonics, aug 1999.

[7] R. J. Wood, S. Avadhanula, R. Sahai, E. Steltz, and R. S. Fearing. Microrobot Design Using Fiber Reinforced Composites. *Journal of Mechanical Design*, 130(5):052304, may 2008.

[8] J P Whitney, P S Sreetharan, K Y Ma, and R J Wood. Pop-up book MEMS. *Journal of Micromechanics and Microengineering*, 21(11):115021, nov 2011.

[9] Sawyer B. Fuller, Alexander Sands, Andreas Haggerty, Michael Karpelson, and Robert J. Wood. Estimating attitude and wind velocity using biomimetic sensors on a microrobotic bee. In *2013 IEEE International Conference on Robotics and Automation*, pages 1374–1380. IEEE, may 2013.

[10] Remo Bruhwiler, Benjamin Goldberg, Neel Doshi, Onur Ozcan, Noah Jafferis, Michael Karpelson, and Robert J. Wood. Feedback control of a legged microrobot with on-board sensing. In *2015 IEEE/RSJ International Conference on Intelligent Robots and Systems (IROS)*, pages 5727–5733. IEEE, sep 2015.

[11] E Farrell Helbling, John A Paulson, and Robert J Wood. A Review of Propulsion, Power, and Control Architectures for Insect-Scale Flapping-Wing Vehicles. 2018.

[12] J. K. Paik, R. K. Kramer, and R. J. Wood. Stretchable circuits and sensors for robotic origami. In *2011 IEEE/RSJ International Conference on Intelligent Robots and Systems*, pages 414–420. IEEE, sep 2011.

[13] Z. E. Teoh, S. B. Fuller, P. Chirarattananon, N. O. Prez-Arancibia, J. D. Greenberg, and R. J. Wood. A hovering flapping-wing microrobot with altitude control and passive upright stability. In *2012 IEEE/RSJ International Conference on Intelligent Robots and Systems*, pages 3209–3216. IEEE, oct 2012.

[14] Xinyan Deng, L. Schenato, Wei Chung Wu, and S.S. Sastry. Flapping flight for biomimetic robotic insects: part I-system modeling. *IEEE Transactions on Robotics*, 22(4):776–788, aug 2006.

[15] Pierre-Emile J. Duhamel, Castor O. Perez-Arancibia, Geoffrey L. Barrows, and Robert J. Wood. Biologically Inspired Optical-Flow Sensing for Altitude Control of Flapping-Wing Microrobots. *IEEE/ASME Transactions on Mechatronics*, 18(2):556–568, apr 2013.

[16] Sylvain Mange, E. Farrell Helbling, Nick Gravish, and Robert J. Wood. An actuated gaze stabilization platform for a flapping-wing microrobot. In *2017 IEEE International Conference on Robotics and Automation (ICRA)*, pages 5409–5414. IEEE, may 2017.

[17] Noah T Jafferis, Michael J Smith, and Robert J Wood. Design and manufacturing rules for maximizing the performance of polycrystalline piezoelectric bending actuators. *Smart Materials and Structures*, 24(6):065023, jun 2015.

[18] Noah T Jafferis, Mario Lok, Nastasia Winey, Gu-Yeon Wei, and Robert J Wood. Multilayer laminated piezoelectric bending actuators: design and manufacturing for optimum power density and efficiency. *Smart Materials and Structures*, 25(5):055033, may 2016.

[19] R.J. Wood, E. Steltz, and R.S. Fearing. Optimal energy density piezoelectric bending actuators. *Sensors and Actuators A: Physical*, 119(2):476–488, apr 2005.

[20] Kevin Y Ma, Pakpong Chirarattananon, Sawyer B Fuller, and Robert J Wood. Controlled flight of a biologically inspired, insect-scale robot. *Science (New York, N.Y.)*, 340(6132):603–7, may 2013.

[21] Neel Doshi, Kaushik Jayaram, Benjamin Goldberg, and Robert J Wood. Phase Control for a Legged Microrobot Operating at Resonance. 2017.

[22] Jeffrey J. Dosch, Daniel J. Inman, and Ephrahim Garcia. A Self-Sensing Piezoelectric Actuator for Collocated Control. *Journal of Intelligent Material Systems and Structures*, 3(1):166–185, jan 1992.

[23] Garnett E. Simmers, Jeffrey R. Hodgkins, David D. Mascarenas, Gyuhae Park, and Hoon Sohn. Improved Piezoelectric Self-sensing Actuation. *Journal of Intelligent Material Systems and Structures*, 15(12):941–953, dec 2004.

[24] Y.G. Cui, Wei Jie Dong, C.Y. Gao, Q.Y. Zeng, and Bao Yuan Sun. Study on Displacement Self-Sensing of Piezoelectric Actuator. *Key Engineering Materials*, 339:240–245, may 2007.

[25] Mohammad N. Islam and Rudolf J. Seethaler. Self-sensing tracking control for piezoelectric actuators based on sensor fusion. volume 8345, page 834541. International Society for Optics and Photonics, apr 2012.

[26] C.-K. Lee. Piezoelectric Laminates. pages 75–167. Springer, Dordrecht, 1992.

[27] D. Campolo, R. Sahai, and R.S. Fearing. Development of piezoelectric bending actuators with embedded piezoelectric sensors for micromechanical flapping mechanisms. In *2003 IEEE International Conference on Robotics and Automation (Cat. No.03CH37422)*, volume 3, pages 3339–3346. IEEE.

[28] Kaushik Jayaram, Noah T Jafferis, Neel Doshi, Ben Goldberg, and Robert J Wood. Concomitant sensing and actuation for piezoelectric microrobots. *Smart Materials and Structures*, 27(6):065028, jun 2018.

[29] Shannon A. Rios, Andrew J. Fleming, and Yuen Kuan Yong. Miniature Resonant Ambulatory Robot. *IEEE Robotics and Automation Letters*, 2(1):337–343, jan 2017.

[30] Wenqi Hu, Guo Zhan Lum, Massimo Mastrangeli, and Metin Sitti. Small-scale soft-bodied robot with multimodal locomotion. *Nature*, 554(7690):81–85, jan 2018.

[31] Yufeng Chen, Neel Doshi, Benjamin Goldberg, Hongqiang Wang, and Robert J. Wood. Controllable water surface to underwater transition through electrowetting in a hybrid terrestrial-aquatic microrobot. *Nature Communications*, 9(1):2495, dec 2018.

[32] Yufeng Chen, Hongqiang Wang, E. Farrell Helbling, Noah T. Jafferis, Raphael Zufferey, Aaron Ong, Kevin Ma, Nicholas Gravish, Pakpong Chirarattananon, Mirko Kovac, and Robert J. Wood. A biologically inspired, flapping-wing, hybrid aerial-aquatic microrobot. *Science Robotics*, 2(11):eaao5619, oct 2017.

[33] Daniel M Aukes, Benjamin Goldberg, Mark R Cutkosky, and Robert J Wood. An analytic framework for developing inherently-manufacturable pop-up laminate devices. *Smart Mater. Struct.*, 23(9):094013, 2014.

[34] Jayant Sirohi and Inderjit Chopra. Fundamental Understanding of Piezoelectric Strain Sensors. *Journal of Intelligent Material Systems and Structures*, 11(4):246–257, apr 2000.

[35] Gustav Gautschi. Piezoelectric Sensors. In *Piezoelectric Sensorics*, pages 73–91. Springer Berlin Heidelberg, Berlin, Heidelberg, 2002.

[36] M A Graule, P Chirarattananon, S B Fuller, N T Jafferis, K Y Ma, M Spenko, R Kornbluh, and R J Wood. Perching and takeoff of a robotic insect on overhangs using switchable electrostatic adhesion. *Science*, 352(6288):978–982, May 2016.

[37] Robert Wood, Radhika Nagpal, and Gu-Yeon Wei. Flight of the robobees. *Sci. Am.*, 308(3):60–65, March 2013.

[38] Mountcastle Andrew M., Helbling E. Farrell, and Wood Robert J. An insect-inspired collapsible wing hinge dampens collision-induced body rotation rates in a microrobot. *J. R. Soc. Interface*, 16(150):20180618, January 2019.

[39] Robert J Wood. The First Takeoff of a Biologically Inspired At-Scale Robotic Insect. *IEEE TRANSACTIONS ON ROBOTICS*, 24(2), 2008.

[40] N Doshi, B Goldberg, R Sahai, N Jafferis, D Aukes, R J Wood, and J A Paulson. Model driven design for flexure-based microrobots. In *Intelligent Robots and Systems (IROS), 2015 IEEE/RSJ International Conference on*, pages 4119–4126, 2015.

[41] Ralph V Cartar. Morphological senescence and longevity: An experiment relating wing wear and life span in foraging wild bumble bees. *J. Anim. Ecol.*, 61(1):225–231, 1992.

[42] Andrew M Mountcastle, Teressa M Alexander, Callin M Switzer, and Stacey A Combes. Wing wear reduces bumblebee flight performance in a dynamic obstacle course. *Biol. Lett.*, 12(6), June 2016.

[43] N T Jafferis, M A Graule, and R J Wood. Nonlinear resonance modeling and system design improvements for underactuated flapping-wing vehicles. In *2016 IEEE International Conference on Robotics and Automation (ICRA)*, pages 3234–3241. ieeexplore.ieee.org, May 2016.